IEEE Access
Multidisciplinary | Rapid Review | Open Access Journal

Received July 25, 2019, accepted August 15, 2019, date of publication August 19, 2019, date of current version October 29, 2019.

Digital Object Identifier 10.1109/ACCESS.2019.2936241

Study on Phase Correction for USCT Echo Image by Sound-Speed Image With Different Resolutions and Noise Levels

XIAOLEI QU[1,2], ZISHENG YAO[1], WENBIN TIAN[1,2], AND JIANGTAO SUN[1,2], (Member, IEEE)

[1]School of Instrumentation and Optoelectronic Engineering, Beihang University, Beijing 100083, China
[2]Beijing Advanced Innovation Center for Big Data-Based Precision Medicine, Beihang University, Beijing 100083, China

Corresponding author: Jiangtao Sun (jiangtao_sun@buaa.edu.cn)

This work was supported in part by Beihang University under Grant KG12114001 and Grant ZG216S1970, and in part by Beihang University under Grant KG12114001 and Grant ZG216S1970.

ABSTRACT Ultrasound computed tomography (USCT) is a promising technique for breast cancer detection. It provides three modalities: sound-speed-image (SSI), attenuation image, and echo image. In these modalities, the echo image is appropriate for the early detection of breast cancer, because it has high resolution. However, echo image reconstruction generally employs an assumed (pre-determined) sound speed to calculate the arrival time of echo signal, the mismatch between the assumed and real sound speeds results in phase aberration of echo signal, and the phase aberration further leads to a decline in image resolution and contrast. To correct the phase aberration, SSI can be used to provide sound speed information instead of the assumed speed, but the resolution of and noise level in SSI may affect the correction performance and echo image quality. In this article, we explored the effect of SSI resolution and the noise level on the resolution and contrast of echo image. First, USCT raw data was obtained by both numerical and experiment studies. Second, echo images were reconstructed by synthetic aperture (SA) technique, and their phase aberration was corrected by multi-stencils fast marching (MSFM) using SSIs with different resolutions and noise levels. Finally, the resolution and contrast of echo images were quantitatively evaluated. Both numerical simulation and phantom experiment demonstrated that the quality of echo images deteriorates as the SSI resolution decreases and the noise level increases.

INDEX TERMS Echo image, phase aberration correction, sound speed image, ultrasound computed tomography.

I. INTRODUCTION

Nowadays, X-ray mammography is widely used as a screening tool for early detection of breast cancer. However, there are three disadvantages in the use of mammography for breast cancer screening. First, women have to suffer ionizing radiation because X-ray is used. Second, it is difficult to detect early breast cancer in women with dense breast, because the overlap of suspicious tissue and glandular tissue on the two-dimensional (2D) mammography images. Finally, women would have to suffer from pain and discomfort, because their breasts need to be compressed during imaging. A recent study [1] reported that mammography with adjunctive ultrasound imaging can significantly enhance the sensitivity for screening of dense breasts. However, current ultrasound imaging techniques suffers from non-isotropic low resolution and high dependence on operator skill, which limited its ability on screening and early detection of breast cancer.

In order to overcome the disadvantages of current techniques, ultrasound computed tomography (USCT) has been proposed as a promising tool for breast cancer screening or diagnosis [2], [3]. It can automatically obtain three-dimensional (3D) breast images with three different modalities, including sound-speed-image (SSI), attenuation image, and echo image [4]–[7]. The USCT imaging system mainly includes a bed with an opening on it, a water tanker under the opening of the bed, and a ring ultrasound transducer immersed in the water tank. The ring transducer is generally composed of thousands of ultrasound elements, and able to be mechanically moved up and down. The USCT imaging procedure is as follows [8], [9]: women or patients for

The associate editor coordinating the review of this article and approving it for publication was Tao Zhou.

imaging lie prone on the bed with one of their breasts naturally drooping through the opening of the bed. Under the opening, the ring transducer encircles the breast in water. Then each element of the ring transducer fires pulse sound wave, while others receive transmissive and echo waves. After that, three modalities of 2D coronal breast images can be reconstructed, and 3D breast images can be obtained by mechanically moving the ring transducer up and down. After receiving raw data, SSI and attenuation images can be reconstructed using the arrival time and amplitude of transmissive wave signal in the raw data. The echo image can then be obtained by synthetic aperture (SA) technique using echo wave signal in the raw data. Generally, the echo image can provide the highest resolution among the three modalities, and therefore it is the most appropriate modality to detect breast cancer in early stages, which always has small size. The quality of echo image, including resolution and contrast ratio (CR), is important for the early detection of breast cancer. However, it always be degraded by phase aberration due to the mismatch between the real and assumed sound speeds for image reconstruction.

Most of ultrasound echo imaging methods, including USCT echo imaging method, generally assume human tissue to be homogenous and employ a pre-determined sound speed for beamforming. However, the real human tissue is not homogenous, and there is a mismatch between the real and pre-determined sound speeds. The mismatch results in the calculation error of delay time of echo wave signal, which is the direct reason for phase aberration [10], [11]. Regarding the current ultrasound echo imaging using linear transducers, a lot of previous studies focused on phase aberration correction. Donnell *et al*. proposed to correlate echo signals obtained from different channels for phase aberration correction [12], [13]. Their method can not only be applied to medical ultrasound imaging but also to any coherent imaging. Levin *et al*. corrected phase aberration of medical ultrasound using speckle brightness as a quality factor [14]. Both Donnell and Levin's methods shifted received signals of each channel and corrected phase aberration by the maximum correlation between channels or brightness of image, but they didn't directly estimate the mismatch between the real and pre-determined sound speeds, which is the root cause for phase aberration. Cho and Yoon used different methods to estimate the average sound speed of tissues, and then corrected phase aberration by using the estimated sound speed instead of the pre-determined one [15], [16]. However, human tissues are inhomogeneous, and there still is a mismatch between the estimated average sound speed and the real sound speed. Because USCT can provide information about the sound speed distribution by the SSI reconstruction. A natural idea is to use the SSI instead of the pre-determined sound speed for the phase aberration correction of echo images. Several previous studies made attempts on this idea [17]–[22]. Ruiter, Qu, and Duric had reconstructed SSIs using straight-ray, bent-ray and full-wave-inversion methods, respectively, and successfully corrected the phase aberration of echo images using the reconstructed SSIs. These three SSI reconstruction methods can give SSIs of different resolution with different computational costs. Also, the noise levels in the reconstructed SSIs strongly depend on the choices of regularization parameter. To understand the effect of SSI resolution on phase correction performance, Ruiter et. al had compared the resolutions of echo images with phase corrected by SSIs with two different resolutions, which were reconstructed by the straight-ray and bent-ray methods [23], [24], respectively. However, two resolutions may be not enough, and it would be better to cover more possible resolutions, because even the bent-ray method can provide SSIs with different resolutions due to the differences in implementation details. Moreover, the effect of the noise level in SSI on the phase correction should also be explored.

Our group had reconstructed SSI by the bent-ray method [25], and then corrected phase aberration of echo image by multi-stencils fast marching (MSFM) method [20] and bent-ray tracing method [21]. Besides, we made efforts to investigate the effect of SSI resolution and the noise level on the correction performance by evaluating the quality of echo images, the phase aberrations of which were corrected using SSIs with possible resolutions. However, in our previous conference paper, we only evaluated the effect of SSI resolution on the resolution of echo image [26]. In this article, we not only evaluated the effect of SSI resolution on both the resolution and contrast of echo image, but also additionally studied the effect of the noise level in SSI on the phase correction and echo image quality.

II. METHODS

A. ECHO IMAGING AND PHASE CORRECTION METHODS

The SA technique is generally employed for echo imaging in USCT. It uses a complete set of raw data from each emitter-receiver pair and allows both dynamic transmit and receive focusing [27], therefore, it can produce high-quality echo images. MSFM is a fast method and can be used to numerically solve the eikonal equation [28], which can provide the sound propagation time regarding the calculation of SSI and correct phase aberration. In this study, the SA was employed as the echo imaging method, and MSFM method was used for phase aberration correction.

Figure 1 shows the schematic diagram of USCT scanning. The ring transducer is composed of thousands of ultrasound elements, each of element emits spherical wave one by one, the wave propagates into the tissue inside the ring, undergoing a complex combination of reflection, refraction, scattering and attenuation, before being received by all other elements. The received raw data can be recorded as $S(t, m, n)$, in which t is received time, m denotes receiver index and n indicates the emitter index. Then the echo image can be reconstructed by:

$$I(\vec{p}) = \sum_{n=1}^{N} \sum_{m=1}^{M} a(m, n)\, S(t(\vec{p}, m, n), m, n) \qquad (1)$$

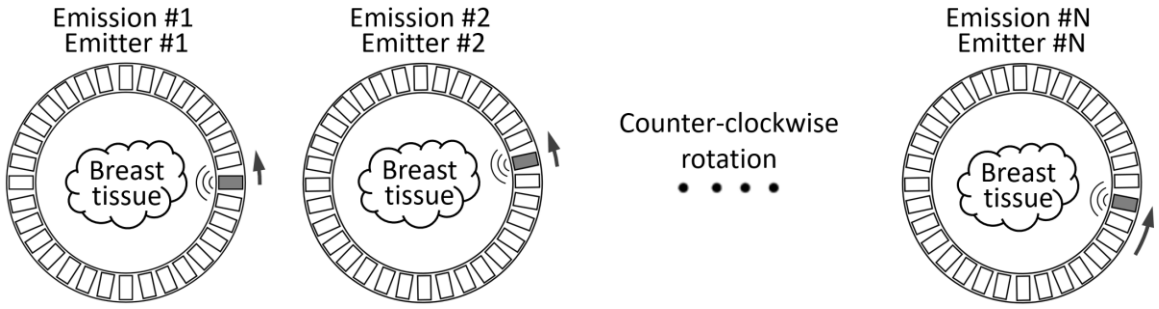

FIGURE 1. Schematic diagram of USCT scanning; USCT: Ultrasound computed tomography.

where, N and M are the emitter and receiver numbers, respectively; $a\,(m, n)$ is apodization function; $t\,(\vec{p}, m, n)$ denotes the sound wave propagation time from emitter n to the position $\vec{p}$, and back to the receiver m.

In conventional ultrasound imaging methods, $t\,(\vec{p}, m, n)$ is calculated using the distance divided by the pre-determined sound speed. The distance is calculated by adding the distance from the emitter n to the position $\vec{p}$ and the distance from position $\vec{p}$ to the receiver m. The mismatch between the real and pre-determined sound speeds results in the calculation error of $t\,(\vec{p}, m, n)$, which directly leads to phase aberration.

In this study, we employed MSFM method to calculate $t\,(\vec{p}, m, n)$ by solving eikonal equation. MSFM method assumes that the wave front evolves by motion in the normal direction, the motion of the front is described by the eikonal equation:

$$\|\Delta T\,(\vec{p})\|\,F\,(\vec{p}) = 1 \tag{2}$$

where T and F are the arrival time and the speed of the front at point $\vec{p}$, respectively, in 2D, the numerical approximation of $\|\Delta T\,(\vec{p})\|$ is given by Godunov:

$$\left[\max(D_{i,j}^{-x}, D_{i,j}^{+x}, 0)\right]^2 + \left[\max(D_{i,j}^{-y}, D_{i,j}^{+y}, 0)\right]^2 = \frac{1}{F_{i,j}^2} \tag{3}$$

where $D_{i,j}^{-}$ and $D_{i,j}^{+}$ are the standard backward and forward finite difference schemes at location (i, j). In MSFM, ΔT is approximated by a second-order finite difference scheme, the equation can be written as:

$$\begin{cases} D_{i,j}^{-x} = \dfrac{3T_{i,j} - 4T_{i-1,j} + T_{i-2,j}}{2} \\ D_{i,j}^{+x} = \dfrac{3T_{i,j} - 4T_{i+1,j} + T_{i+2,j}}{2} \\ D_{i,j}^{-y} = \dfrac{3T_{i,j} - 4T_{i,j-1} + T_{i,j-2}}{2} \\ D_{i,j}^{+y} = \dfrac{3T_{i,j} - 4T_{i,j+1} + T_{i,j+2}}{2} \end{cases} \tag{4}$$

Additionally, MSFM also uses the information provided by diagonal point to improve numerical accuracy along diagonal direction [28]. It can track the evolution of an expanding front with high accuracy. By using MSFM, the motion of the wave front from a given pixel position (ultrasound element position) can be trace, and the arrival time of the wave front at each pixel can be calculated, considering both sound speed distribution and sound wave refraction. Our group has successfully corrected phase aberration of USCT by using MSFM in our previous studies [20], [21].

B. NUMERICAL SIMULATION AND PHASE CORRECTION EVALUATION

In this sub-section, we will introduce the numerical simulation and give the procedure to evaluate the effect of SSI resolution and the noise level on the phase aberration correction and image quality.

The numerical simulation was conducted by an open-source acoustics toolbox (K-wave simulation toolbox), which was developed by Treeby and Cox [29] and designed for time domain acoustic and ultrasound simulation in complex and tissue-realistic media. In our simulation, the diameter of USCT ring transducer was 100 mm, which was the same as our experiment prototype. The ring transducer was composed of 1024 elements. The central frequency of the fired pulse wave was 1.6 MHz, and the sampling frequency of the received raw data was set to be 10 MHz.

For investigating the effect of SSI resolution and the noise level on the phase correction, we evaluated the resolution and contrast of echo images, which were reconstructed using SSIs with different resolutions and noise levels. As shown in Figure 2, there are mainly four steps in our numerical evaluation process. First, speed models were established; second, USCT raw data was simulated for resolution and contrast evaluation; Third, SSIs with different resolutions were obtained by applying mean filters of different size to the speed models, and we got SSIs with different noise levels by adding gaussian noises with different standard deviations to the speed models; Finally, echo images were reconstructed by SA technique and then their respective resolution and contrast were quantitatively evaluated.

Regarding speed models preparation, we selected 2D MRI slices of breast, including adipose, glandular and skin regions, from 3D MRI breast images of nine patients with diverse breast features. Then, we segmented the selected slices into adipose, glandular, skin and background regions

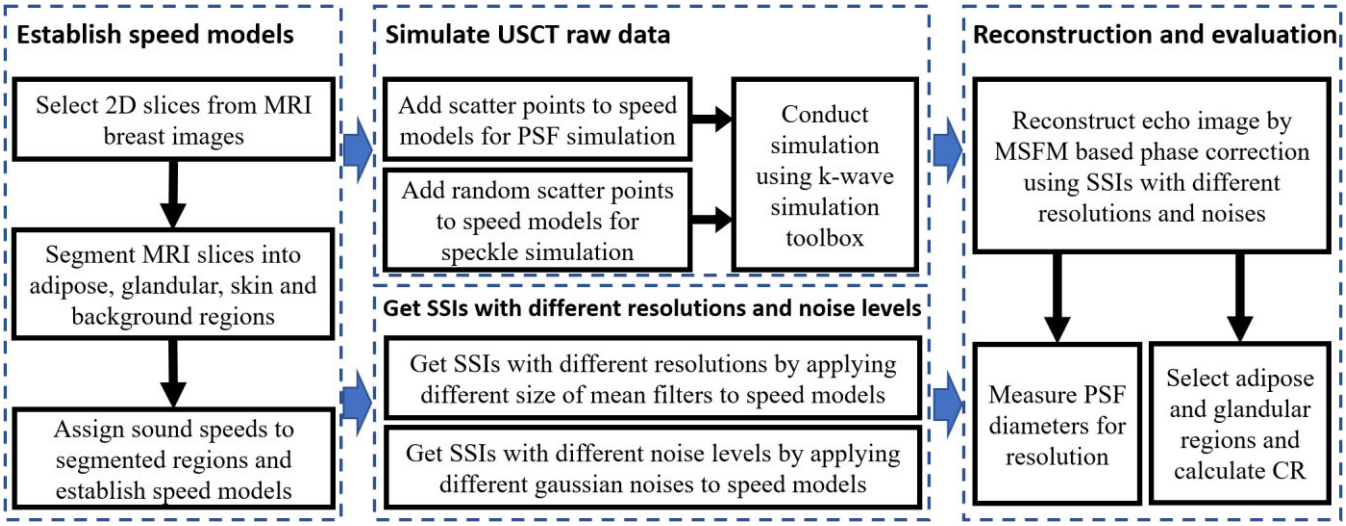

FIGURE 2. Flow chat for evaluating phase correction in numerical simulation; USCT: Ultrasound computed tomography; SSI: Sound-speed-image; PSF: Point spread function; CR: Contrast ratio.

by a modified OTSU threshold method. After segmentation, we assigned sound speeds of 1470, 1570, 1600 and 1540 m/s to the segmented adipose, glandular, skin and background regions, respectively. Then, we prepared nine 2D speed models, including speed distribution information, for the numerical simulation.

In the simulation, we simulated two kinds of raw data for resolution and contrast evaluations, respectively. For resolution evaluation, we need to measure the diameters of PSF. Therefore, we placed 5×5 scatter points in the speed models with interval of 10 mm and diameter of 0.1 mm. These scatter points had an extremely different impedance (2000 m/s for sound speed and 2000 kg/m^3 for density) to the speed models, which made the segmentation and their diameter measurement easy to implement in echo images. For contrast evaluation, we added random scatter points to adipose and glandular tissue, respectively. After adding random scatter points, the values of sound speed for adipose and glandular regions were 1470 ± 1.47 and 1570 ± 7.85 m/s (mean $\pm$ standard deviation, 1.47 is 0.1% of 1470, and 7.85 is 0.5% of 1570), respectively. The random variation and scatter points resulted in speckle and different intensities in adipose and glandular regions of echo images, which made contrast evaluation possible.

Regarding image reconstruction and evaluation, we reconstructed echo images and evaluated its resolution and contrast. The echo images were reconstructed by SA technique. Their phase aberrations were corrected by MSFM using SSIs with different resolutions and noise levels. For resolution evaluation, the images of scatter points were segmented by the threshold of half the local maximum, then we assumed that the echo image had isotropic resolutions, and the segmented region was circular, the diameter of which can be considered as the diameter of PSF. For contrast evaluation, we manually selected adipose and glandular regions from echo images with random scatter points and calculated CR by [30]:

$$CR = 20log_{10}\left(\frac{\mu_g}{\mu_a}\right) \tag{5}$$

where μ_a and μ_g are the mean intensity values of adipose and glandular regions.

C. PHANTOM EXPERIMENT AND PHASE CORRECTION EVALUATION

In phantom experiment, we built an USCT prototype. It had similar parameters to that in the numerical simulation. The ring transducer was composed of 1024 elements, the central frequency of each element was 1.6 MHz. As Figure 3 shows, the ring transducer was connected to an ultrasound open platform with 256 channels (Verasonics, Inc., Kirkland, WA, USA) with a multiplexer, and the sampling frequency was set to be 10 MHz. For scanning, the ring transducer surrounded a breast mimic phantom. During scanning, both the transducer and phantom were immersed in shallow water, which guaranteed that the sound wave was able to propagate through water into breast phantom. The phantom was part of a whole breast phantom. We trimmed it to fit into the ring transducer (100 mm diameter). Even its shape didn't look like breast, but it still had glandular-mimic structure inside.

To evaluate the effect of SSI resolution and the noise level on phase aberration correction in phantom experiment, there were mainly five steps as shown in Figure 4. First, we obtained raw data in the breast-mimic phantom experiment. Second, we reconstructed SSI by the bent-ray tracing method [31]. Third, we smoothed SSI using mean filters with different sizes (approximate 1, 10, 20, 30, 40, 50, 60, 70, 80, 90, 100 mm), and added gaussian noises with different standard deviations to SSI. The mean value of gaussian noise is 0 and its standard deviation ranges from 0 to 100 m/s with 10 m/s as the interval. Then we obtained SSIs with different

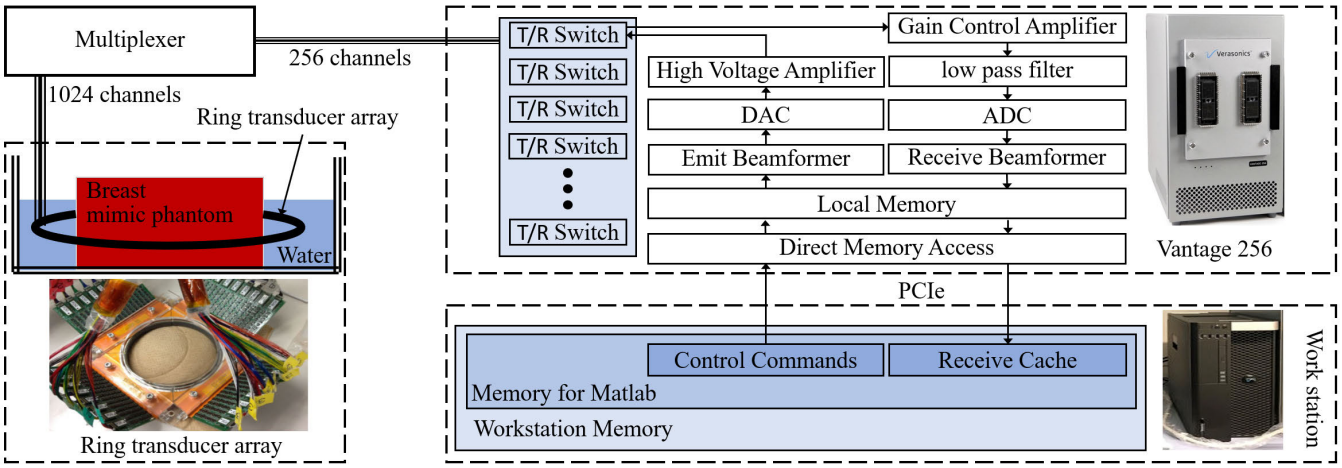

FIGURE 3. Phantom experiment setup.

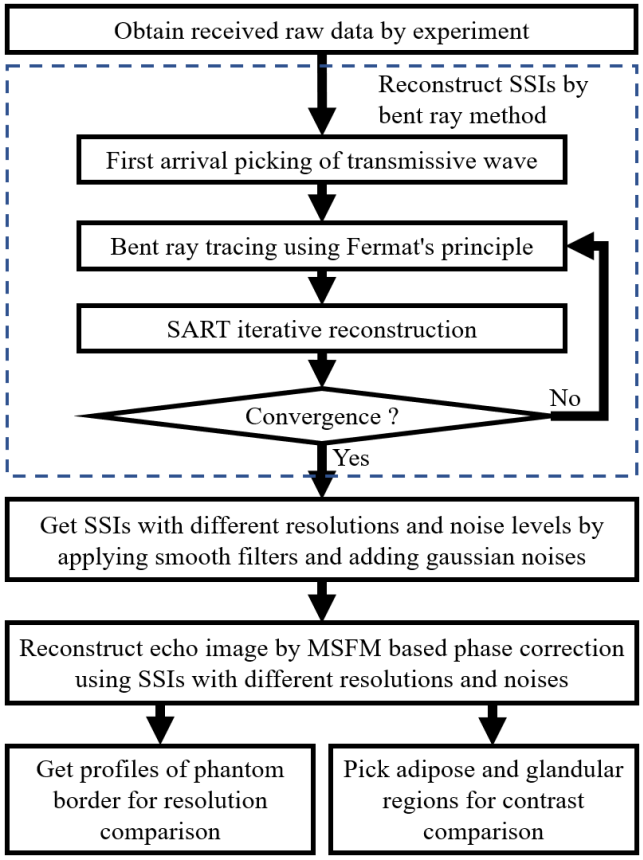

FIGURE 4. Flow chat for evaluating phase correction in phantom experiment; SSI: Sound-speed-image; SART: Simultaneous algebraic reconstruction technique; MSFM: Multi-stencils fast marching.

resolutions and noise levels. Fourth, we reconstructed echo images by SA technique and corrected their phase aberration by MSFM method using SSIs with different resolutions and noise levels. Finally, we evaluated and compared the reconstructed echo images. Specifically, we qualitatively compared intensity profiles of images along the edge of breast phantom for resolution evaluation, and we quantitively examine CRs of images by manually picking adipose and glandular regions for contrast evaluation.

Regarding SSI reconstruction, the bent-ray method was employed. As Figure 4 shows, there were mainly four steps. First, the first arrival time of transmissive wave was picked up by using the Akaike information criterion (AIC) method [32]. Second, the bent ray between each pair of emitter and receiver was calculated with the current SSI by applying Fermat's principle [31]. At the first iteration, a pre-determined sound speed distribution was assigned to initialize SSI. Third, SSI was reconstructed and updated by simultaneous algebraic reconstruction technique (SART) [33]. Fourth, if the difference between the SSIs before and after the third step was sufficiently small, we considered that the iteration was convergent, and the SSI reconstruction was completed. But, if the difference was large, the reconstruction process went back to the second step for the next iteration.

III. RESULTS

A. SIMULATION RESULTS

Figure 5 shows the speed models for numerical simulation, which were obtained by segmenting breast MRI images of nine women and assigning the sound speed of 1540, 1600, 1470, and 1570 m/s to water, skin, adipose and glandular regions. The speed models were zoomed out to fit into the ring transducer with 100 mm in dimeter, which had the same size as our small prototype of ring transducer. These breast models had different shapes, sizes and breast densities (ratio of glandular to adipose tissue). The breast in Figure 5(b) is small, but those in Figure 5(e) and (f) are large. The breast in Figure 5(h) has low density, but that in Figure 5(e) obviously has higher density.

For resolution evaluation, we placed scatter points with an extremely higher sound speed (2000 m/s) and a small size (square shape with 0.1mm side-length) in the sound speed model. Figure 6(a) gives an example of sound speed models

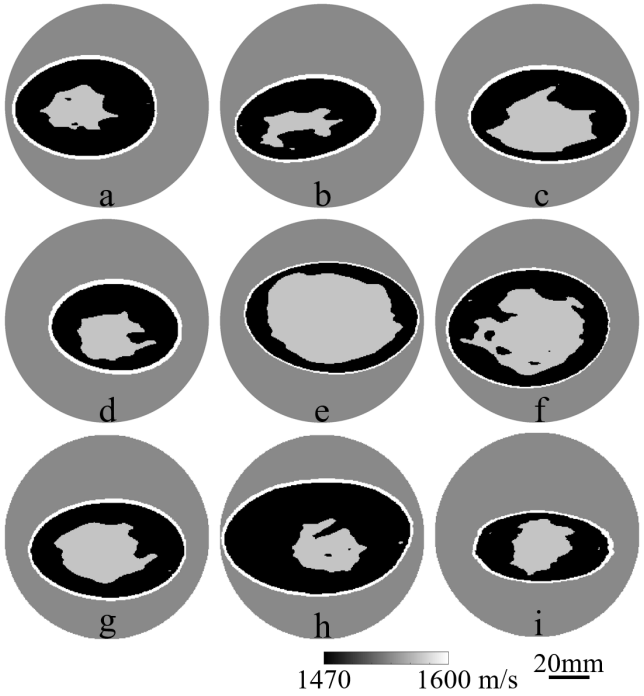

FIGURE 5. Sound speed models for numerical simulation. (a)-(i) were obtained by segmenting MRI breast images of nine women, respectively. MRI: Magnetic resonance imaging.

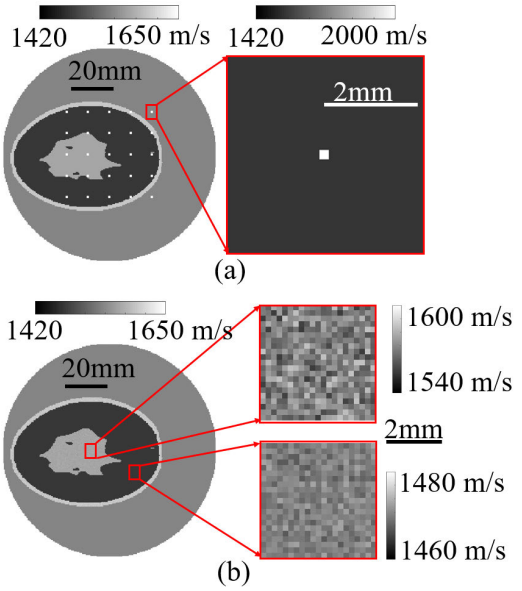

FIGURE 6. Speed models for resolution and contrast evaluation. (a) Speed model with sparse scatter points for resolution evaluation. (b) Speed model with random scatter points for contrast evaluation.

with sparse scatter points for resolution evaluation. There are 5×5 scatter points, which were placed in the center of the models with an interval of 10 mm. For contrast evaluation, we placed random scatter points in adipose and glandular tissue regions. Figure 6(b) gives an example of sound speed models with random scatter points. The values of sound speeds in adipose and glandular tissue regions were 1470 m/s with 0.1% in standard deviation and 1570 m/s with 0.5% in standard deviation, which made the intensity of glandular tissue region was higher than that of adipose tissue region.

Figure 7 shows SSIs for phase aberration correction, which had different resolutions and noise levels. The SSIs with different resolutions were obtained by applying mean filters of different size to the sound speed model (Figure 5(a)). The sizes of mean filters to obtain Figure 7(a), (b), and (c) were 0.2, 40, and 100 mm, respectively. In Figure 7(a), the SSI resolution is high, and the details of breast tissue can be observed, since the size of mean filter is quite small. In Figure 7(b), the image is quite blur, but a low-speed region due to the adipose of breast can still be recognized. In Figure 7(c), the image almost only shows the average sound speed in the imaging region, because its filter size is 100 mm which is equal to the diameter of the imaging region. The SSIs with different noise levels were obtained by adding gaussian noises with different standard deviations. The standard deviations in Figure 7(d) and (e) are 50 and 100 m/s, respectively.

Figure 8 shows the reconstructed echo images. Their phase aberrations were corrected using SSIs with different resolutions and noise levels. Figure 8(a)-(c) and (g)-(i) show the

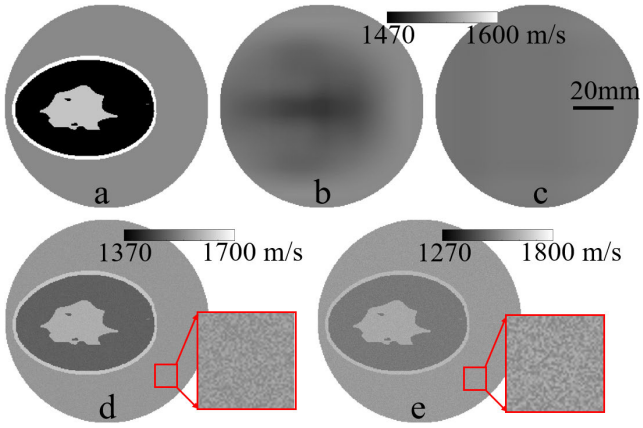

FIGURE 7. SSIs for phase aberration correction. (a)-(c) are obtained by applying mean filters to sound speed models, and sizes of these filters are 0.2, 40, and 100 mm, respectively. (d) and (f) are obtained by adding gaussian noises to (a), with SDs of 50 and 100 m/s, respectively. SSI: Sound-speed-image; SD: Standard deviation.

reconstructed echo images with sparse scatters for resolution evaluation. In these images, the contours of skin, adipose and glandular regions can be clearly observed, because different regions had been assigned different sound speeds and impedances in the numerical simulation model. Comparing to these contours, the scatter points had been assigned extremely different sound speeds and impedances, thus they had higher intensities and can easily be segmented from the contours and background, which provided convenience for the diameter measurement of scatter points (PSF diameter). Figure 8(d)-(f) and (j)-(l) give the reconstructed echo images with random scatters for contrast evaluation. In these images, not only the contours of adipose and glandular regions can be

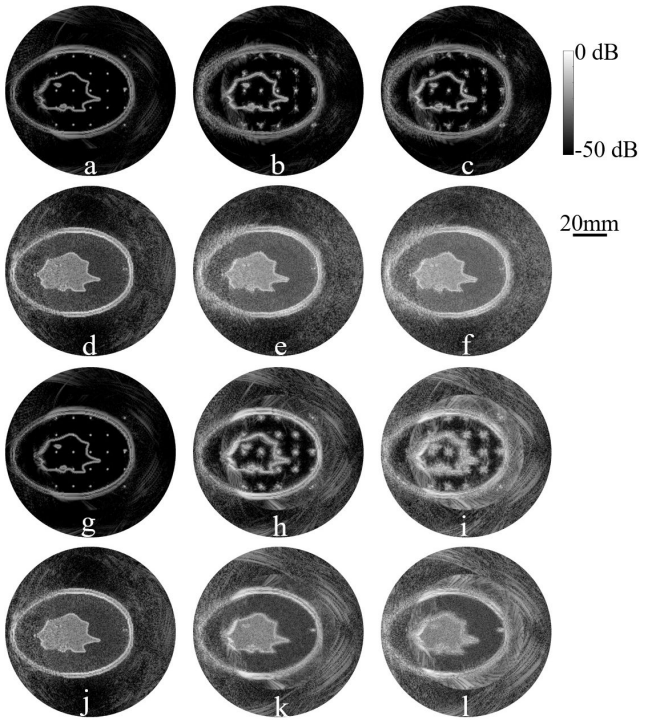

FIGURE 8. Reconstructed echo images for resolution ((a)-(c) and (g)-(i) with sparse scatters) and contrast ((d)-(f) and (j)-(l) with random scatters) evaluations. (a)-(f) were reconstructed using SSIs, which were smoothed by mean filters of 0.2 ((a) and (d)), 40 ((b) and (e)), and 100 ((c) and (f)) mm. (g)-(l) were reconstructed using SSIs, to which gaussian noises were added, with standard deviations of 0 ((g) and (j)), 50 ((h) and (k)), and 100 ((i) and (l)) m/s.

observed, but also the intensities of these two regions were different, because the standard deviation of sound speeds in the two regions were different, which were 1.47 m/s and 7.85 m/s, respectively. The different intensities of these two regions can be used to calculate CR by Equation 5 for quantitative contrast evaluation.

Figure 9 quantitatively demonstrates the effect of SSI resolution and the noise level on the echo image quality (resolution and contrast), which indicates the performance of phase correction. In Figure 9(a), the diameters of PSF increase as the mean filter size increases. In Figure 9(b), the diameter of PSF in each case increases as the standard deviation of gaussian noise increases. Figure 9(a) and (b) denotes the higher resolution of and lower noise level in SSI can provide echo images with higher resolutions. In Figure 9(c), the CR decreases as the mean filter size increases. In Figure 9(d), the CR decreases as the standard deviation of gaussian noise increases. Figure 9(c) and (d) denotes the higher resolution of and lower noise level in SSI can give echo images with higher CRs. Figure 9 quantitatively demonstrates that the higher resolution of and lower noise level in SSI can improve the phase correction performance.

The numerical simulation results show that the resolution and CR of reconstructed echo image are indeed affected by the resolution of and noise level in the SSI used for phase correction. Furthermore, they also give the quantitative

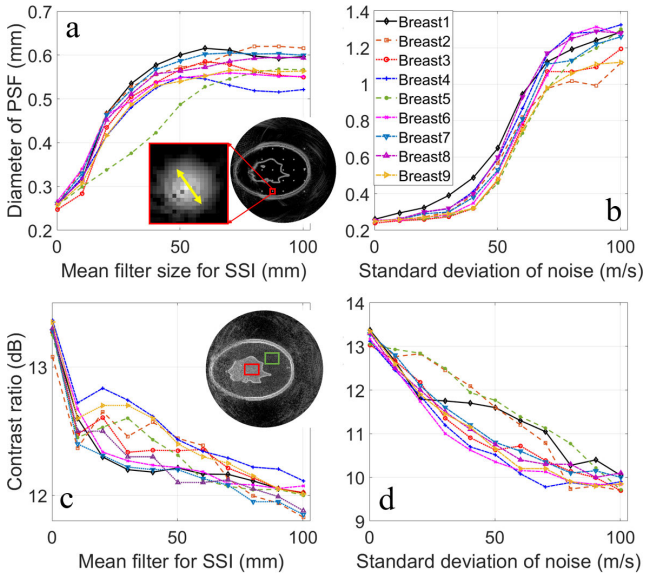

FIGURE 9. PSF diameter and CR of echo images. (a) and (b) are PSF diameters affected by resolution of and noise level in SSI, respectively. (c) and (d) are CR affected by resolution of and noise level in SSI, respectively. CR: Contrast ratio; PSF: Point spread function; SSI: Sound-speed-image.

relationship between the quality of echo image (resolution and contrast) and the quality of SSI (resolution and noise level) used for phase correction.

B. EXPERIMENTAL RESULTS

Figure 10(a) shows our experiment setup. A piece of breast phantom, which was cut from a whole breast phantom, was hanged inside the ring transducer. Both breast phantom and

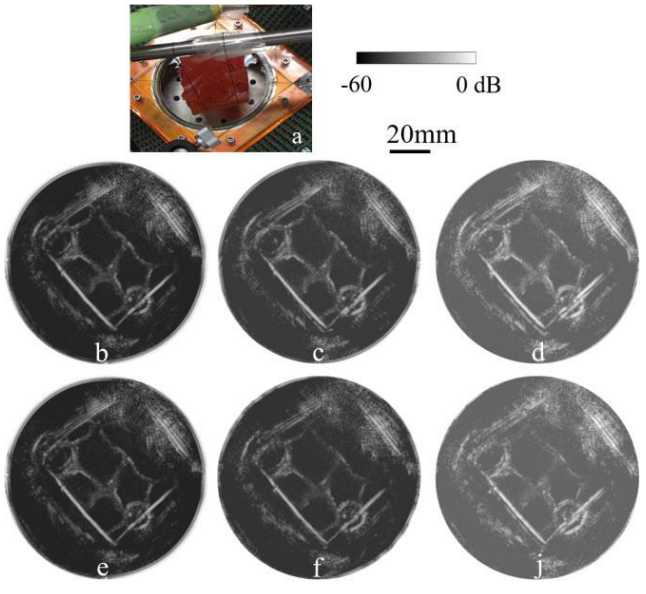

FIGURE 10. Experiment setup and reconstructed echo images. (a) experiment setup. (b)-(d) are echo images reconstructed using SSIs, which are smoothed by mean filters of 5, 50, and 100 mm, respectively. (e)-(j) are reconstructed using SSIs, to which gaussian noises are added, with standard deviations of 0, 50, and 100 m/s, respectively.

ring transducer were immersed in shallow degassed water. Figure 10(b)-(j) shows the reconstructed echo images. Their phase aberrations were corrected using SSIs. The SSIs for Figure 10(b)-(d) were obtained by applying mean filters with sizes of 5, 50, and 100 mm to the reconstructed SSI, respectively. The SSIs for Figure 10(e)-(j) were obtained by adding gaussian noises with standard deviations of 0, 50, and 100 m/s, respectively.

Figure 11(a) and (b) show the intensity profiles of echo images along the border of the breast phantom marked with red line. They qualitatively demonstrate that the width of phantom border in echo images is smaller when the SSI for phase correction has higher resolution and lower noise level. Figure 11(c) and (d) quantitatively show that CR of echo image decreases with the increase in the mean filter size or the standard deviation of noise. This is consistent with the observation in echo images (Figure 10) and indicates that the echo image contrast became worse when the SSI for phase correction has lower resolution or higher noise level. Figure 11 demonstrates that the resolution of and noise level in SSI do affect the performance of phase correction, and the phase correction will be better when the resolution of SSI increases or the noise level decreases.

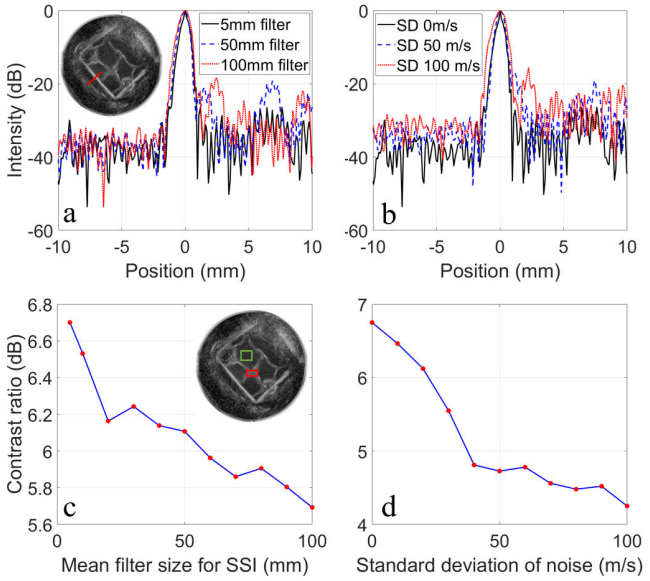

FIGURE 11. Intensity profiles along border of phantom and CR of echo images. (a) and (b) are intensity profiles along red line in echo images; (c) and (d) are CRs between red and green regions in echo images. SD: Standard deviation; SSI: Sound-speed-image.

IV. DISCUSSION

In this study, we conducted numerical simulation and phantom experiment to investigate the effect of SSI resolution and the noise level on the performance of phase correction. When the resolution of SSI decreases (i.e. the mean filter size applied on SSI increases) or the noise level in SSI increases, the calculation error of propagation time from each element to each pixel increases, which results in poorer phase correction performance and image quality. The numerical simulation results quantitatively demonstrated that the diameter of PSF increased and CR between adipose and glandular tissue regions decreased when the resolution of SSIs for phase correction decreased or the noise level in SSI increased. The experimental results qualitatively showed that the width of breast phantom border in echo images increased (indicating that the resolution of echo image decreased) and CR in echo image decreased, when the resolution of SSI decreased or the noise level increased. Reductions in both the resolution and CR indicated that the phase correction performance was degraded, when SSI had lower resolution or higher noise level.

In the simulation, we applied mean filters and added noises to sound speed models to generate desired SSIs and study their effect on the phase correction. However, this was different from real application scenarios and our experimental study. In the real scenario or experiment, we can only reconstruct SSIs but can't obtain the sound speed model. Figure 12 (a) and (b) give the reconstructed SSI from the simulation data corresponding to the sound speed model in Figure 5(a) and the experimental data, respectively. Compared to the sound speed model, Figure 12(a) has lower resolution, but contains low-level noises, because of the use of bent ray method and SART for SSI reconstruction. For evaluation under the conditions resembling the experimental and real application scenarios, we also applied mean filter and added noises to the reconstructed SSIs from the simulation data. Figure 13 shows the PSF diameters and CRs of echo images. The resolution and CR of each echo image in Figure 13 are worse than their counterparts in Figure 9, when applying mean filters of small size and adding low-level noises, but almost the same, when applying filter of large size and adding high-level noises. The resolution of reconstructed SSI from the experimental data is lower than that of the corresponding sound speed model, which would lead to a significant deterioration of phase correction performance, when the applied mean filter is of small size and added noise is of low-level, but a negligible deterioration, when the mean filter is of large size and noise is of high-level.

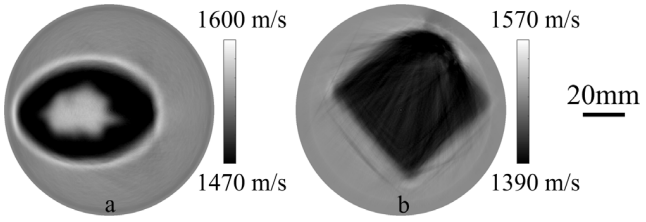

FIGURE 12. SSIs reconstructed by bent-ray method. (a) SSI from simulation data. (b) SSI from experiment data. SSI: Sound-speed-image.

The simulation results also showed that the PSF diameter of echo image obtained with the ring transducer might be smaller than half of the ultrasound wavelength. Since the central frequency was 1.6 MHz, half of the wavelength should be approximate 0.48 mm with the sound speed of 1540 m/s,

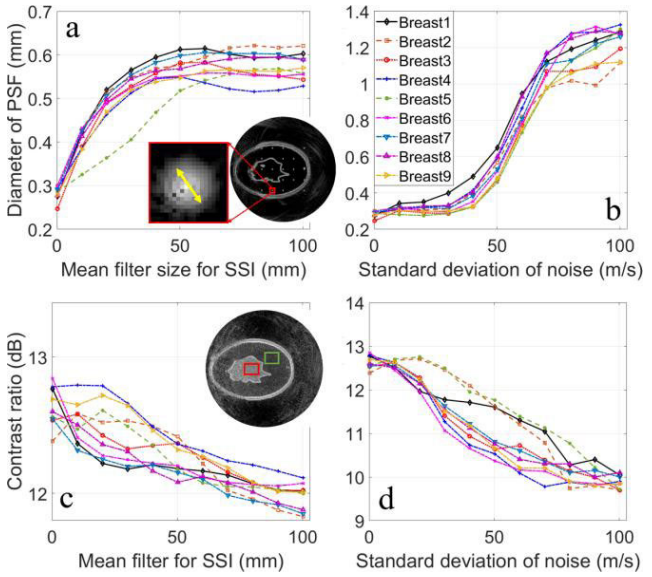

FIGURE 13. **PSF diameter and CR of echo images using reconstructed SSI for phase correction. (a) and (b) are PSF diameters affected by resolution of and noise level in SSI, respectively. (c) and (d) are CR affected by resolution of and noise level in SSI, respectively. CR: Contrast ratio; PSF: Point spread function; SSI: Sound-speed-image.**

but the PSF diameter was even smaller than 0.3 mm in Figure 9. The reason may be that beamforming can be implemented at all directions, when using the ring transducer. This may be an interesting study to be conducted in the future.

V. CONCLUSION

In this article, we studied the phase correction for USCT echo image by using SSI with different resolutions and noise levels. It was demonstrated that the phase correction performance decreased as the resolution of SSI decreased or the noise level in SSI increased. The numerical simulation gave the quantitative relationship between the quality of echo image (resolution and CR) and the quality of used SSI for phase correction (resolution and noise level). When the resolution of SSI changed from 0.2 to 100 mm, the PSF diameter of echo image increased from 0.3 to 0.6 mm and the CR decreased from 13.5 to 12.0 dB approximately. When the standard deviation of noise in SSI changed from 0 to 100 m/s, the PSF diameter of echo image increased from 0.3 to 1.2 mm and the CR decreased from 13.5 to 10.0 dB approximately. The phantom experiment further validated the relationship. It was qualitatively showed that the resolution of echo image decreased when the SSI resolution decreased or the noise level in SSI increased. Moreover, it was quantitatively illustrated that the CR of echo image decreased as the resolution of SSI decreased or the noise level increased. In summary, this study quantitatively evaluated the effect of SSI resolution and the noise level on the phase correction for USCT echo image.

ACKNOWLEDGMENT

X. Qu would like to thank Prof. Azuma at the University of Tokyo for providing phantom and experiment equipment.

REFERENCES

[1] N. Ohuchi, A. Suzuki, T. Sobue, M. Kawai, S. Yamamoto, Y.-F. Zheng, Y. N. Shiono, H. Saito, S. Kuriyama, E. Tohno, T. Endo, A. Fukao, I. Tsuji, T. Yamaguchi, Y. Ohashi, M. Fukuda, and T. Ishida, "Sensitivity and specificity of mammography and adjunctive ultrasonography to screen for breast cancer in the Japan strategic anti-cancer randomized trial (J-START): A randomised controlled trial," *Lancet*, vol. 387, no. 10016, pp. 341–348, Jan. 2016.

[2] N. Duric, P. Littrup, S. Schmidt, C. Li, O. Roy, L. Bey-Knight, R. Janer, D. Kunz, X. Chen, J. Goll, A. Wallen, F. Zafar, V. Allada, E. West, I. Jovanovic, K. Li, and W. Greenway, "Breast imaging with the SoftVue imaging system: First results," *Proc. SPIE*, vol. 8675, Mar. 2013, Art. no. 86750K.

[3] H. Gemmeke, T. Hopp, M. Zapf, C. Kaiser, and N. V. Ruiter, "3D ultrasound computer tomography: Hardware setup, reconstruction methods and first clinical results," *Nucl. Instrum. Methods Phys. Res. A, Accel. Spectrom. Detect. Assoc. Equip.*, vol. 873, pp. 59–65, Nov. 2017.

[4] N. V. Ruiter, M. Zapf, T. Hopp, H. Gemmeke, K. W. A. van Dongen, J. Camacho, J. L. Herraiz, M. P. Liva, and J. M. Udías, "USCT reference data base: Conclusions from the first SPIE USCT data challenge and future directions," *Proc. SPIE*, vol. 10580, Mar. 2018, Art. no. 105800Q.

[5] C. Li, N. Duric, P. Littrup, and L. Huang, "*In vivo* breast sound-speed imaging with ultrasound tomography," *Ultrasound Med. Biol.*, vol. 35, no. 10, pp. 1615–1628, Oct. 2009.

[6] N. V. Ruiter, M. Zapf, T. Hopp, R. Dapp, and H. Gemmeke, "Phantom image results of an optimized full 3D USCT," *Proc. SPIE*, vol. 8320, Feb. 2012, Art. no. 832005.

[7] K. Wang, T. Matthews, F. Anis, C. Li, N. Duric, and M. A. Anastasio, "Waveform inversion with source encoding for breast sound speed reconstruction in ultrasound computed tomography," *IEEE Trans. Ultrason., Ferroelectr., Freq. Control*, vol. 62, no. 3, pp. 475–493, Mar. 2015.

[8] N. V. Ruiter, T. Hopp, M. Zapf, E. Kretzek, and H. Gemmeke, "Analysis of patient movement during 3D USCT data acquisition," *Proc. SPIE*, vol. 9790, Apr. 2016, Art. no. 979009.

[9] N. Duric, P. Littrup, O. Roy, C. Li, S. Schmidt, X. Cheng, and R. Janer, "Clinical breast imaging with ultrasound tomography: A description of the SoftVue system," *J. Acoust. Soc. Amer.*, vol. 135, no. 4, p. 2155, Apr. 2014.

[10] M. Karaman, A. Atalar, H. Köymen, and M. O'Donnell, "A phase aberration correction method for ultrasound imaging," *IEEE Trans. Ultrason., Ferroelectr., Freq. Control*, vol. 40, no. 4, pp. 275–282, Apr. 1993.

[11] Y. Li, "Phase aberration correction using near-field signal redundancy—Part I: Principles," *IEEE Trans. Ultrason., Ferroelectr., Freq. Control*, vol. 44, no. 2, pp. 355–371, Mar. 1997.

[12] S. W. Flax and M. O'Donnell, "Phase-aberration correction using signals from point reflectors and diffuse scatterers: Basic principles," *IEEE Trans. Ultrason., Ferroelectr., Freq. Control*, vol. UFFC-35, no. 6, pp. 758–767, Nov. 1988.

[13] M. O'Donnell and S. W. Flax, "Phase-aberration correction using signals from point reflectors and diffuse scatterers: Measurements," *IEEE Trans. Ultrason., Ferroelectr., Freq. Control*, vol. UFFC-35, no. 6, pp. 768–774, Nov. 1988.

[14] L. Nock, G. E. Trahey, and S. W. Smith, "Phase aberration correction in medical ultrasound using speckle brightness as a quality factor," *J. Acoust. Soc. Amer.*, vol. 85, no. 5, pp. 1819–1833, May 1989.

[15] M. H. Cho, L. H. Kang, J. S. Kim, and S. Y. Lee, "An efficient sound speed estimation method to enhance image resolution in ultrasound imaging," *Ultrasonics*, vol. 49, no. 8, pp. 774–778, Dec. 2009.

[16] C. Yoon, Y. Lee, J. H. Chang, T.-K. Song, and Y. Yoo, "*In vitro* estimation of mean sound speed based on minimum average phase variance in medical ultrasound imaging," *Ultrasonics*, vol. 51, no. 7, pp. 795–802, Oct. 2011.

[17] N. V. Ruiter, R. Schnell, M. Zapf, and H. Gemmeke, "P3D-2 phase aberration correction for 3D ultrasound computer tomography images," in *Proc. IEEE Ultrason. Symp.*, Oct. 2007, pp. 1808–1811.

[18] E. Kretzek, R. Dapp, M. Zapf, M. Birk, and N. V. Ruiter, "Evaluation of phase aberration correction for a 3D USCT using a ray trace based simulation," in *Proc. IEEE Int. Ultrason. Symp. (IUS)*, Jul. 2013, pp. 378–381.

[19] E. Kretzek and N. V. Ruiter, "GPU based 3D SAFT reconstruction including phase aberration," *Proc. SPIE*, vol. 9040, Mar. 2014, Art. no. 90400W.

[20] X. Qu, T. Azuma, H. Lin, H. Imoto, S. Tamano, S. Takagi, S.-I. Umemura, I. Sakuma, and Y. Matsumoto, "Phase aberration correction by multi-stencils fast marching method using sound speed image in ultrasound computed tomography," *Proc. SPIE*, vol. 9790, Apr. 2016, Art. no. 979018.

[21] X. Qu, S. Fan, and T. Azuma, "Phase aberration correction by bent-ray tracing method for ultrasound computed tomography," in *Proc. IEEE Int. Conf. Imag. Syst. Techn. (IST)*, Oct. 2017, pp. 1–6.
[22] S. Schmidt, N. Duric, C. Li, O. Roy, and Z.-F. Huang, "Modification of Kirchhoff migration with variable sound speed and attenuation for acoustic imaging of media and application to tomographic imaging of the breast," *Med. Phys.*, vol. 38, no. 2, pp. 998–1007, Feb. 2011.
[23] T. Hopp, M. Zapf, H. Gemmeke, and N. V. Ruiter, "Experimental evaluation of straight ray and bent ray phase aberration correction for USCT SAFT imaging," *Proc. SPIE*, vol. 10580, Mar. 2018, Art. no. 105800M.
[24] T. Hopp, F. Zuch, M. Zapf, H. Gemmeke, and N. V. Ruiter, "Experimental analysis of ray-based sound speed reconstruction algorithms for phase aberration corrected USCT SAFT imaging," *Proc. SPIE*, vol. 10955, Mar. 2019, Art. no. 109550J.
[25] X. Qu, T. Azuma, H. Lin, H. Nakamura, S. Tamano, S. Takagi, S.-I. Umemura, I. Sakuma, and Y. Matsumoto, "Computational cost reduction by avoiding ray-linking iteration in bent-ray method for sound speed image reconstruction in ultrasound computed tomography," *Jpn. J. Appl. Phys.*, vol. 56, no. 7S1, Jun. 2017, Art. no. 07JF14.
[26] X. Qu, S. Fan, Z. Yao, S. Gao, J. Sun, S. Zhang, and T. Azuma, "The effect of sound-speed-image resolution on phase aberration correction for ultrasound computed tomography," in *Proc. IEEE Int. Conf. Imag. Syst. Techn. (IST)*, Oct. 2018, pp. 1–5.
[27] X. Qu, T. Azuma, T. Yogi, S. Azuma, H. Takeuchi, S. Tamano, and S. Takagi, "Synthetic aperture ultrasound imaging with a ring transducer array: Preliminary ex vivo results," *J. Med. Ultrason.*, vol. 43, no. 4, pp. 461–471, Oct. 2016.
[28] M. S. Hassouna and A. A. Farag, "Multistencils fast marching methods: A highly accurate solution to the Eikonal equation on Cartesian domains," *IEEE Trans. Pattern Anal. Mach. Intell.*, vol. 29, no. 9, pp. 1563–1574, Sep. 2007.
[29] B. E. Treeby and B. T. Cox, "K-Wave: MATLAB toolbox for the simulation and reconstruction of photoacoustic wave fields," *Proc. SPIE*, vol. 15, no. 2, Mar. 2010, Art. no. 021314.
[30] M. A. Lediju, G. E. Trahey, B. C. Byram, and J. J. Dahl, "Short-lag spatial coherence of backscattered echoes: Imaging characteristics," *IEEE Trans. Ultrason., Ferroelectr., Freq. Control*, vol. 58, no. 7, pp. 1377–1388, Jul. 2011.
[31] A. H. Andersen, "A ray tracing approach to restoration and resolution enhancement in experimental ultrasound tomography," *Ultrason. Imag.*, vol. 12, no. 4, pp. 268–291, 1990.
[32] C. Li, L. Huang, N. Duric, H. Zhang, and C. Rowe, "An improved automatic time-of-flight picker for medical ultrasound tomography," *Ultrasonics*, vol. 49, no. 1, pp. 61–72, Jan. 2009.
[33] A. H. Andersen and A. C. Kak, "Simultaneous algebraic reconstruction technique (SART): A superior implementation of the art algorithm," *Ultrason. Imag.*, vol. 6, no. 1, pp. 81–94, 1984.

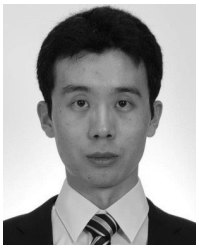

XIAOLEI QU was born in Pucheng, China, in 1984. He received the B.E. degree in software engineering from Xi'an Jiaotong University, Xi'an, China, in 2007, the M.S. degree in pattern recognition from the Huazhong University of Science and Technology, Wuhan, China, in 2009, and the Ph.D. degree in bioengineering from The University of Tokyo, Japan, in 2012.

From 2012 to 2014, he was a Senior Engineer with the Techwin Research Center, Samsung Group, Fukuoka, Japan. From 2014 to 2017, he was a Project Researcher with The University of Tokyo. Since 2017, he has been an Associate Professor with the School of Instrumentation and Optoelectronic Engineering, Beihang University, Beijing, China. He is the author of more than 20 articles. He holds four patents. His research interests include medical ultrasound imaging, image processing, and recognition.

ZISHENG YAO was born in Fuzhou, China, in 1995. He received the B.E. degree in measurement and control technology and instrumentation from Beihang University, Beijing, China, in 2018, where he is currently pursuing the master's degree with the School of Instrumentation and Optoelectronic Engineering. Since 2018, he has been a Trainee Engineer of instrument control and measurement with the China Instrument and Control Society. His research interests include ultrasound imaging, non-destructive testing technology, and optimization methods for inverse problems.

WENBIN TIAN received the B.Eng. degree in electrical engineering from Sichuan University, China, in 2011, and the M.Sc. degree in microwave and communication engineering from The University of Manchester, U.K., in 2013, and the Ph.D. degree from the School of Electrical and Electronic Engineering, The University of Manchester, U.K., in 2018. He currently holds a postdoctoral position at Beihang University, Beijing, China. His current research interest include electrical tomography and ultrasound computed tomography, sensor design, and image processing.

JIANGTAO SUN received the B.Eng. and M.Eng. degrees in measurement and control technology and instrument from Xidian University, Shanxi, China, in 2008 and 2010, respectively, and the Ph.D. degree in electrical and electronic engineering from The University of Manchester, Manchester, U.K., in 2014. In 2014, he joined the Brunel Innovation Centre, The Weld Institute, Brunel University London, as a Research Fellow. Thereafter, from 2016 to 2017, he was an Associate Professor in biomedical engineering with Sun Yat-sen University, China. He is currently an Associate Professor in instrumentation science with Beihang University, China. His current research interest includes electrical tomography and ultrasound computed tomography for industrial and biomedical applications.